J. Phys. Chem. 1988, 92, 2913–2925

Vibrational Spectroscopy of Hydrogen Cyanide Clusters

Deon S. Anex, Ernest R. Davidson, Constantine Douketis, and George E. Ewing*

Department of Chemistry, Indiana University, Bloomington, Indiana 47405

(Received: October 6, 1987)

Molecular beams of monomer HCN and its clusters, generated by supersonic helium expansions, were crossed with the output of an F-center laser operating in the C–H stretching region. The laser was scanned in its low-resolution mode, $\Delta\nu_{1/2} = 10$ GHz (0.3 cm^{-1}), from 3100 to 3400 cm^{-1} while the molecular beam energy was monitored with a liquid helium cooled bolometer. Excitation spectra of monomer HCN and vibrational photofragmentation spectra of HCN clusters were recorded. Bands associated with unresolved vibration–rotation envelopes were assigned to dimer and trimer transitions. Features corresponding to tetramers and higher polymers were observed but remain unassigned. Under some expansion conditions a photofragmenting solidlike hydrogen cyanide feature was observed. A band corresponding to one of the bound C–H stretching vibrations in the linear trimer was studied under high resolution (15 MHz). For the few comparisons possible, our C–H stretching frequencies are in agreement with other gas-phase measurements. Our results are also consistent with matrix isolation studies when allowances are made for the large solvent shifts possible. Three theoretical approaches were used to predict trends in the C–H stretching frequencies on hydrogen bonding. These are normal-coordinate analysis, a classical electrostatic model, and ab initio quantum mechanics calculations. A critique of these theoretical models is presented. Finally, the observed vibrational predissociation lifetime of the linear trimer is discussed in terms of simple propensity rules.

Introduction

Clusters of hydrogen cyanide provide an excellent series for tracing the development of properties in a hydrogen-bonded system from the dimer, through higher polymers, to aggregates large enough to exhibit solidlike properties. These properties include structural aspects, such as cluster geometries and intermolecular and intramolecular bond lengths. Spectroscopic features and rates of dynamic processes such as vibrational predissociation may be observed as aggregates grow. The HCN system also has potentially a simple geometry, since it tends to form linear complexes. Linear dimer and trimer have been observed in rotational,[1–3] and vibrational[4–6] spectroscopic studies. It has been speculated that there may also be higher linear polymers.[4,7] The propensity of hydrogen cyanide to form linear complexes is also supported by the high dielectric constant of the liquid.[8,9] Finally, X-ray studies show that the solid may be regarded as a collection of infinite hydrogen-bonded linear chains oriented parallel to each other.[10] Although HCN has a tendency for linear complex formation, nonlinear geometries are also possible. For example, the infrared spectrum of a cyclic trimer has been observed.[6] Additionally, recent ab initio calculations show the cyclic tetramer to be slightly more stable than the linear tetramer.[7]

The present investigation of HCN and its complexes is a continuation of the spectroscopic study of gas-phase dimers and trimers[11] in general, and of those involving hydrogen bonding in particular.[12] A common theme in these studies has been the relation between gas-phase properties and condensed phases.[13] In recent years beam techniques have provided many avenues for the study of weakly bound species. The results, however, have the shortcoming of congestion due to various size complexes which often obscures information on a species of a particular size. Typically the infrared absorptions due to various clusters are often only slightly shifted as the cluster size grows.[14] Consequently dimer and higher polymer features are badly overlapped. In some cases a clear view of the spectra of the dimer species may be obtained once the beam composition has been carefully adjusted to exclude higher order polymers;[15] however, the size-selective study of higher clusters is more difficult.

The richness of hydrogen-bonded systems is illustrated by the studies of HF clusters. The dimer, $(HF)_2$, has been investigated in the microwave region[16] and in the infrared, both in the bulk gas[17] and in a molecular beam.[18] A bent, open chain structure has been established. The line widths indicate an interesting difference in vibrational predissociation rates depending on whether the free or bound H–F stretching mode is excited.[17–19] The vibrational predissociation spectrum of trimer, $(HF)_3$, has also recently been obtained by using isotopic substitution in conjunction with mass spectroscopic detection.[20] The infrared spectrum of solid HF has been recorded,[21] demonstrating a red shift even larger than that of the gas-phase dimer or trimer features. Many other hydrogen-bonded species have been studied[12] including those containing HCN.

The spectroscopy of hydrogen-bonded complexes of HCN has received recent attention. The rotational spectrum of dimer $(HCN)_2$ and its ^{15}N-substituted isotopes has been studied,[1–3] establishing the linear geometry. A portion of the vibration–rotation spectrum has been observed in a long path length cooled bulk gas absorption experiment.[5] The resolved rotational structure is consistent with the linear geometry found in the microwave studies and was used to further define spectroscopic constants. The excited-state vibrational predissociation lifetime was obtained from the line width in this bulk gas study. Larger HCN polymers formed in a supersonic expansion have been investigated by using coherent Raman (CARS) and infrared techniques.[4] From this work the trimer, $(HCN)_3$, was suggested to be linear from band contour analysis of a feature in the C–N stretching region. The linear structure was confirmed by microwave spectroscopy.[38] Also

---

* To whom correspondence should be addressed.

(1) Buxton, L. W.; Campbell, E. J.; Flygare, W. H. *Chem. Phys.* **1981**, *56*, 399.
(2) Georgiou, K.; Legon, A. C.; Millen, D. J.; Mjoberg, P. J. *Proc. R. Soc. London A* **1985**, *A399*, 377.
(3) Fillery-Travis, A. J.; Legon, A. C.; Willoughby, L. C.; Buckingham, A. D. *Chem. Phys. Lett.* **1983**, *102*, 126.
(4) Maroncelli, M.; Hopkins, G. A.; Nibler, J. W.; Dyke, T. R. *J. Chem. Phys.* **1985**, *83*, 2129.
(5) Wofford, B. A.; Bevan, J. W.; Olsen, W. B.; Lafferty, W. J. *J. Chem. Phys.* **1986**, *85*, 105.
(6) Jucks, K. W.; Miller, R. E. *J. Chem. Phys.*, submitted for publication.
(7) Kofranek, M.; Karpfen, A.; Lischka, H. *Chem. Phys.* **1987**, *113*, 53.
(8) Coates, G. E.; Coates, J. E. *J. Chem. Soc.* **1944**, *77*.
(9) Pauling, L. *The Nature of the Chemical Bond*; Cornell University Press: Ithaca, NY, 1948.
(10) Dulmage, W. J.; Lipscomb, W. N. *Acta Crystallogr.* **1951**, *4*, 330.
(11) Celli, F. G.; Janda, K. C. *Chem. Rev.* **1986**, *86*, 507.
(12) Legon, A. C.; Millen, D. J. *Chem. Rev.* **1986**, *86*, 635.
(13) Miller, R. E.; Watts, R. O.; Ding, A. *Chem. Phys.* **1984**, *83*, 155.
(14) Gough, T. E.; Miller, R. E.; Scoles, G. *J. Phys. Chem.* **1981**, *85*, 4041.
(15) Jucks, K. W.; Huang, Z. S.; Dayton, D.; Miller, R. E. *J. Chem. Phys.* **1987**, *86*, 4341.
(16) Howard, B. J.; Dyke, T. R.; Klemperer, W. *J. Chem. Phys.* **1984**, *81*, 5417.
(17) Pine, A. S.; Lafferty, W. J. *J. Chem. Phys.* **1983**, *78*, 2154.
(18) Huang, Z. S.; Jucks, K. W.; Miller, R. E. *J. Chem. Phys.* **1986**, *85*, 3338.
(19) DeLeon, R. L.; Muenter, J. S. *J. Chem. Phys.* **1984**, *80*, 6092.
(20) Micheal, D. W.; Lisy, J. M. *J. Chem. Phys.* **1986**, *85*, 2528.
(21) Sastri, M. L. M.; Hornig, D. F. *J. Chem. Phys.* **1963**, *39*, 3497.

0022-3654/88/2092-2913$01.50/0

located by the CARS study were broad features associated with the dimer, trimer, and larger polymers in the C–H stretching region. Recently, infrared molecular beam studies have revealed a rotationally resolved spectrum of the cyclic trimer of HCN as well as high-resolution spectra of the linear dimer and trimer.[6] This high-resolution work has also provided line-width measurements of individual vibration–rotation transitions for the linear dimer and trimer. HCN complexes have also been studied in solid matrices.[22-26] The infrared and Raman spectra of the liquid and of two crystalline phases of the solid are also available.[27-29]

Hydrogen-bonded complexes involving HCN have also been explored theoretically. At the simplest level, normal-coordinate analysis has been used to explore how the vibrational frequencies of the clusters are influenced by the hydrogen bond that holds the HCN monomer units together.[4,22] The structures and infrared spectra of $(HCN)_n$, with $n = 1$–5, for linear and cyclic geometries have been investigated by ab initio quantum mechanical methods.[7] The same properties have also been calculated for an infinite linear chain of HCN.[30] These studies provide a smooth path from monomer through solid properties. The frequency shifts of the C–H stretching vibration upon complexation have been predicted on the basis of isolated monomer electrostatic properties for several binary complexes involving HCN, including $(HCN)_2$.[31]

The present study concentrates on the infrared absorptions in the C–H stretching region studied through vibrational photofragmentation spectroscopy. The frequency of the C–H oscillator in the $(HCN)_n$ cluster is sensitive to cluster size and to its position within a particular cluster. In this paper the experiment is described and the results are presented. Next, the assignment of features is discussed. The results are then compared to other gas-phase and matrix studies. This is followed by the calculation of the vibrational frequency shifts with emphasis on the role of complex size, geometry, and oscillator position within a cluster. First, a normal-mode analysis is considered. Next, a classical electrostatic model[32] is applied. Finally, the experimental results are compared with ab initio quantum mechanical calculations.[7,30] In each of these experimental and theoretical views, attention is paid to the convergence from monomer properties to those of the solid. The vibrational predissociation lifetime is then calculated for the linear trimer by using simple propensity rules and is compared to the value obtained from experimental line-width measurements.

Experimental Section

The molecular beam apparatus is based on the bolometric techniques developed by the Waterloo group.[33] Mixtures of hydrogen cyanide (Fumico) in helium were expanded through a 50-μm-diameter nozzle. Several hydrogen cyanide concentrations were used, ranging from 0.1 to 5 mol %. The concentrations were confirmed by comparing the mass spectrum and the infrared absorption spectrum to those of a carefully prepared standard mixture. The stagnation pressures were varied up to 830 kPa. A skimmer with a 250-μm-diameter opening located about 1 cm from the nozzle collimated the expansion to form the molecular beam. This skimmer separated the source chamber (10^{-3} Torr) from the detector chamber (10^{-6} Torr). From the skimmer, the beam traveled 75 cm to a 1.5 K liquid helium cooled sapphire–germanium composite bolometer (Infrared Labs). The detector area, 2 mm × 2 mm, defined the size of the molecular beam interrogated. The demonstrated detector noise equivalent power was 6×10^{-13} W Hz$^{-1/2}$ and the sensitivity was 3×10^5 V W^{-1} under the conditions of our experiments. This corresponds to being able to detect a flux of $\approx 5 \times 10^6$ vibrationally excited HCN molecules per second.

About 30 cm from the skimmer, the molecular beam was crossed with the output of an F-center laser (Burleigh FCL20). With the internal etalon removed, the laser operated on the fundamental and spatial hole burning modes. These lasing modes are separated by about 10 GHz and are tuned in discrete 300-MHz steps, corresponding to the cavity mode spacing, by rotation of the grating. When band contour information was needed the discrete nature of the scan was smoothed by piezoelectrically translating the folding mirror in the laser cavity. A 20-ms 1-kV ramp caused a rapid scan of the cavity modes across ~2 GHz which averaged the scanning frequency over several cavity mode spacings during the grating scan. This resulted in two laser lines with effective widths of 2 GHz, spaced by 10 GHz. The RbCl:Li crystal was pumped with 1.4 W (all lines, near 647.1 nm) from a krypton ion laser (Spectra Physics Model 171). The frequency calibration of the laser grating position was achieved by recording the absorption spectrum of a bulk sample of hydrogen cyanide gas[34] and is accurate to ±0.5 cm^{-1}. The laser power changed from 12 to 17 mW in scanning from 3100 to 3400 cm^{-1} due to the variation in the gain profile of the laser.

The F-center laser was also operated in its high-resolution mode by inserting the internal etalon into the laser cavity. In this mode the laser line width is 1 MHz, which is effectively broadened to 15 MHz when the multipass arrangement is used, due to the slightly different Doppler shift for each laser–molecular beam crossing. In the high-resolution spectra obtained for this study the frequency was scanned by varying the length of the laser cavity using the piezoelectrically translated folding mirror while simultaneously scanning the spacing of the internal etalon. Individual 1.5-GHz cavity scans were pieced together to form a complete spectrum. Advances in frequency for each cavity scan relative to the previous one were monitored by using a 7.5-GHz spectrum analyzer. In addition, a 10.2-cm sapphire rod was used as a low finesse frequency marker during the cavity scan which aided in piecing the spectrum together as well as monitoring the continuity and spectral quality of the scan.

The molecular beam was flanked by parallel gold-coated optical flats to increase the number of laser–molecular beam crossings. This multipass scheme increased the efficiency of molecular excitation by a factor of 20 compared to a single laser crossing. The laser light was chopped at 83 Hz and the bolometer signal was detected by using a lock-in amplifier (Ithaco Model 393) after a ×1000 preamplifier. Spectra were obtained by monitoring the output of the lock-in amplifier with a strip chart recorder while the laser frequency was scanned.

Results

Through the resistance change in its sapphire–germanium element on heating or cooling, the bolometer monitors the total energy content of the molecular beam impinging upon it. This total energy is the sum of contributions from translational, rotational, and vibrational motions of the atoms and molecules within the beam. A molecule vibrationally excited in the beam by the laser will carry this internal energy to the bolometer and deposit it there if the molecule excited-state lifetime is comparable to or longer than the flight time to the bolometer (≈0.4 ms). This results in a heating of the sapphire–germanium element; a corresponding lowering of its resistance, and a negative going signal as presented in Figures 1 and 2. Alternatively, an excited species that undergoes vibrational predissociation on a timescale fast compared to the flight time results in a cooling of the bolometer due to the depletion of the collimated molecular beam by recoil of the fragments. The bolometer signal in this case is registered

---

(22) Walsh, B.; Barnes, A. J.; Suzuki, S.; Orville-Thomas, W. J. *J. Mol. Spectrosc.* **1978**, *72*, 44.
(23) King, C. M.; Nixon, E. R. *J. Chem. Phys.* **1968**, *48*, 1685.
(24) Pacansky, J. *J. Phys. Chem.* **1977**, *81*, 2240.
(25) Knozinger, E.; Kollhoff, H. *J. Chem. Phys.* **1986**, *85*, 4881.
(26) Knozinger, E.; Wittenbeck, R. *Ber. Bunsenges. Phys. Chem.* **1982**, *86*, 742.
(27) Pezolet, M.; Savoie, R. *Can. J. Spectrosc.* **1972**, *17*, 39.
(28) Pezolet, M.; Savoie, R. *Can. J. Chem.* **1969**, *47*, 3041.
(29) Friedrich, H. B.; Krause, P. F. *J. Chem. Phys.* **1973**, *59*, 4942.
(30) Karpfen, A. *Chem. Phys.* **1983**, *79*, 211.
(31) Liu, S.-Y.; Dykstra, C. E., personal communication.
(32) Liu, S.-Y.; Dykstra, C. E. *J. Phys. Chem.* **1986**, *90*, 3097.
(33) Gough, T. E.; Miller, R. E.; Scoles, G. *Appl. Phys. Lett.* **1977**, *30*, 338.

(34) *Tables of Wavenumbers for the Calibration of Infra-red Spectrometers*; Butterworths: Washington, DC, 1961.

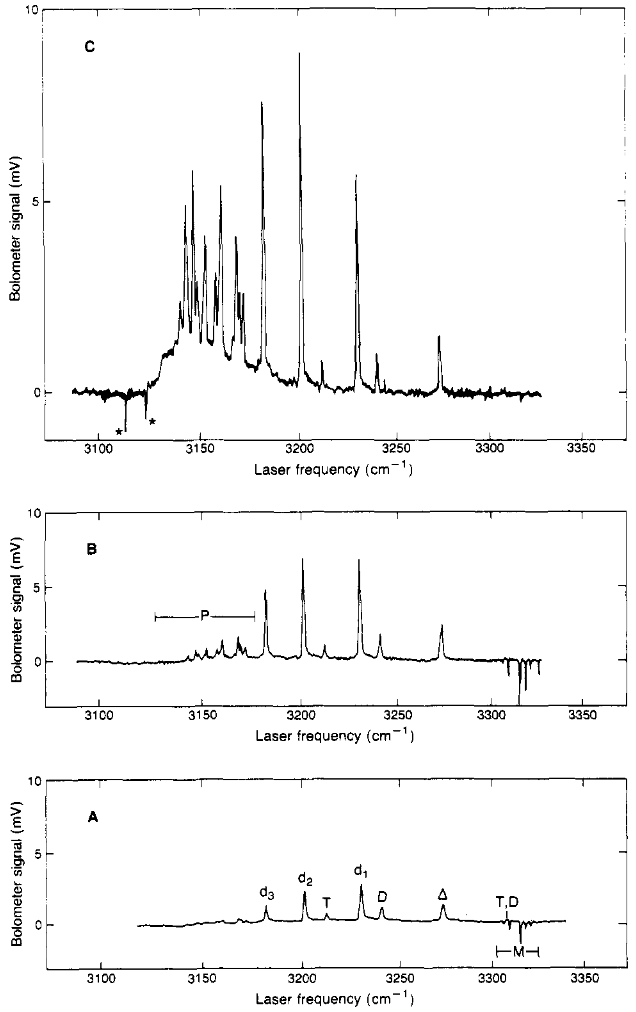

Figure 1. HCN cluster vibrational spectra. For all three panels the gas mixture was 0.4% HCN:He, with stagnation pressures of 380 kPa for (A), 450 kPa for (B), and 790 kPa for (C). The labels M, D, T, and Δ indicate monomer, linear dimer, linear trimer, and cyclic trimer features, respectively. Three prominent diffuse and unassigned features are labeled d_1, d_2, and d_3, with higher polymers labeled P. (The asterisks indicate nonreproducible instrumental artifacts.)

in the positive direction of Figures 1 and 2. Laser excitation of the molecular beam in our experiments, depending on the wavelength, can result in either heating or cooling of the bolometer.

Five spectra representing different stagnation pressures and concentrations of hydrogen cyanide–helium mixtures are presented in Figures 1 and 2. The evolution of the hydrogen cyanide spectra as conditions are made progressively more favorable for polymer formation is seen in Figures 1A–C and 2A,B. In the bottom panel, Figure 1A, representing the lowest hydrogen cyanide concentration and helium backing pressure, the region labeled M is readily assigned to the five monomer HCN vibration–rotation features P(2), P(1), R(0), R(1), and R(2). These features, also appearing in Figure 1B, are the only negative-going signals in the spectra. All other features are positive-going signals and appear at lower frequencies than the band center of the monomer HCN transitions. We shall associate these features with vibrational predissociation transitions of hydrogen cyanide clusters.

The cluster sizes associated with the multitude of features can be assessed by following their relative band strengths with variations in stagnation pressure. At the lowest concentration and stagnation pressure, Figure 1A, the D or $(HCN)_2$ features are present as are two T or linear $(HCN)_3$ features and one feature assigned to the cyclic trimer which is labeled with the triangle (Δ). A dimer and a linear trimer feature overlap near the monomer absorptions. The two dimer features, the cyclic trimer, and a trimer feature at 3306.8 cm^{-1} have been rotationally resolved by Jucks and Miller.[6,47] Our high-resolution spectrum, Figure 3, reveals a second trimer feature at 3212.5 cm^{-1}. Also appearing in Figure 1A are three diffuse bands labeled d_1, d_2, and d_3. Moving to Figure 1B the diffuse features d_1, d_2, and d_3 dominate and a new collection of features labeled P make their first appearance. The P features represent $(HCN)_n$ polymers, perhaps tetramer and larger. In Figure 1C, at roughly twice the stagnation pressure in Figure 1B, the band area of the region labeled P now dominates the overall spectrum while the peak heights of d_1, d_2, and d_3 remain high. Note that in comparing the relative rates of appearance for the three features d_1, d_2, and d_3 in parts A, B, and C of Figure 1, d_3 grows faster than d_2 and d_2 in turn grows faster than d_1. In Figure 2A, with higher HCN concentration, the diffuse feature labeled S appears. We will associate this band with vibrational predissociation of solid hydrogen cyanide since its frequency, 3130.5 cm^{-1}, and band shape coincide with the infrared absorption of the low-temperature phase of the neat crystal.[27] Polymer features, P, now surpass the d_1, d_2, and d_3 peak heights, and monomer, dimer, and trimer features visible in Figure 1A are no longer visible. Finally, in the spectrum for the highest HCN concentration, Figure 2B, the solid feature (S) has disappeared as have the other sharp features leaving only a broad peak centered at 3159 cm^{-1} with a 30-cm^{-1} full width at half-height.

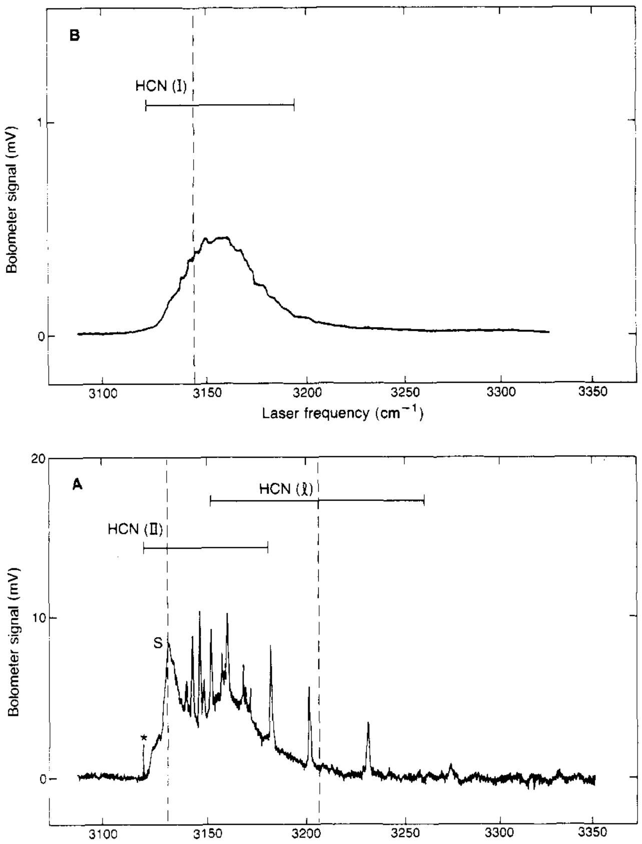

Figure 2. HCN cluster vibrational spectra. For (A) the gas mixture is 2% HCN:He with a 720-kPa stagnation pressure. For (B) 5% HCN:He was expanded from 450 kPa. The location of the peak absorbances from ref 27 of three bulk phases of HCN are indicated by the vertical dashed lines. These phases are the low-temperature crystalline phase (II), the high-temperature crystalline phase (I), and the liquid at −5 °C (l). Widths of these features in the bulk samples are given by the horizontal bars. (The asterisks indicate nonreproducible instrumental artifacts.)

The frequencies, $\tilde{\nu}$ (cm^{-1}), of the hydrogen cyanide spectroscopic features are grouped according to their degree of clustering in Table I. Also listed are the frequency shifts $\Delta\tilde{\nu}$ (cm^{-1}) of these features relative to the band center of monomer HCN at 3311.5 cm^{-1}.[35] In the following discussions of cluster transitions, we will often give both frequency and shifts written as $\tilde{\nu}(\Delta\tilde{\nu})$. The ex-

---

[35] Choe, J. I.; Tipton, T.; Kukolich, S. G. *J. Mol. Spectrosc.* **1986**, *117*, 292.

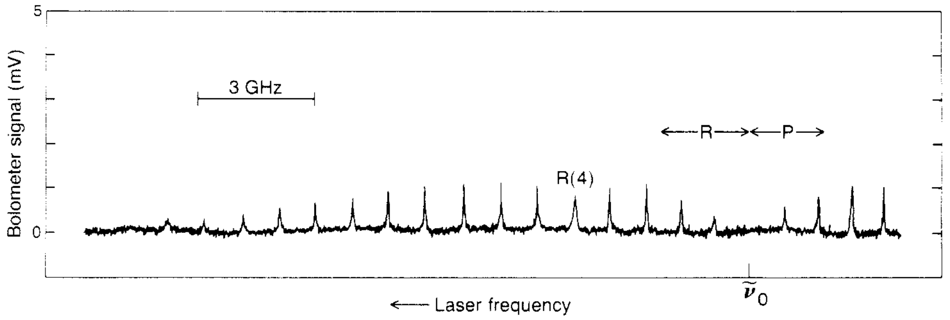

Figure 3. High-resolution spectrum of linear $(HCN)_3$ ν_3. The band center, $\tilde{\nu}_0$, is at 3212.5 cm^{-1}.

TABLE I: Vibrational Frequencies of $(HCN)_n$

feature	$\tilde{\nu}(\Delta\tilde{\nu})^a$	$\tilde{\nu}(\Delta\tilde{\nu})^b$	assignment
M	3311.5 (0.0)^c	3311.5 (0.0)^c	monomer
D	3307.8 (−3.7)^d	3308.0 (−3.5)^e	linear dimer ν_1
D	3241.3 (−70.2)	3241.6 (−69.9)^f	linear dimer ν_2
T	3307.8 (−3.7)^d	3306.8 (−4.7)^g	linear trimer ν_1
T			linear trimer ν_2
T	3212.5 (−99.0)		linear trimer ν_3
Δ	3273.6 (−37.9)	3273.9 (−37.6)^g	cyclic trimer ν_2
d_1	3231.0 (−80.5)		
d_2	3201.7 (−109.8)		
d_3	3182.5 (−129.0)		
P	3171 (−141)		
P	3169 (−143)		
P	3168 (−144)		
P	3159 (−153)		
P	3158 (−154)		
P	3157 (−155)		
P	3151 (−161)		
P	3148 (−164)		
P	3146 (−166)		
P	3142 (−170)		
P	3139 (−173)		
S	3130.5 (−181.0)		solidlike cluster (HCN(II))

[a] In cm^{-1}, this work. [b] In cm^{-1}, literature. [c] Reference 35. [d] ν_1 for linear dimer and trimer overlap. [e] Reference 47. [f] Reference 5. [g] Reference 6.

perimental results together with a stick spectrum are also presented in Figure 5A.

The three features d_1, d_2, and d_3 have been scanned with the laser running in the single-frequency high-resolution mode. At the resolution of the instrument (15 MHz) no structure is resolved. The 3212.5-cm^{-1} (−99.0-cm^{-1}) trimer region, however, reveals rotational fine structure, of which the entire R-branch with a portion of the P-branch is shown in Figure 3. The 3-GHz frequency reference was obtained from a frequency marker which was in turn calibrated against the P(8)–P(9) spacing in gas-phase HCN. By comparison to this reference the full width at half-height of the individual lines averages 60 ± 10 MHz with an anomalous 130 ± 20 MHz width for R(4). The intensity distribution of the spectrum is described by a rotational temperature of 1.4 K.

Discussion

A. Assignment of Spectroscopic Features. Let us consider the assignment of the dimer features in more detail. For linear $(HCN)_2$ there are two infrared allowed C–H stretching vibrations. In the simplest model, these vibrations are uncoupled. One mode is localized in the hydrogen-bonded or donor C–H; the other mode is isolated in the free C–H. In keeping with the well-known trend on self-association, the hydrogen-bonded C–H stretching frequency is expected to be red-shifted relative to the monomer transition. The free C–H stretching vibration is predicted to be less perturbed. Wofford et al.,[5] in a high-resolution study of the bulk gas, have recorded a multitude of vibration–rotation features that they have established to arise from transitions of linear $(HCN)_2$. The band center is located at 3241.6 cm^{-1} (−69.9 cm^{-1}) and, from its considerable red shift, was assigned to ν_2, the hydrogen-bonded C–H stretching vibration. Since this feature coincides with one of our most prominent D features we assume we have observed the same transition and accordingly have entered the assignment in Table I. Maroncelli et al.[4] using CARS spectroscopy on a supersonic beam containing hydrogen cyanide have also found this dimer feature. Because of interfering transitions, neither the high-resolution bulk gas study nor the CARS beam experiment has located the other dimer C–H stretching vibration. Recently, however, a high-resolution molecular beam study has located the $(HCN)_2$ free C–H stretching vibration at 3308.0 cm^{-1} (−3.5 cm^{-1}).[47] The same group has also reported the free C–H stretching vibration for the linear trimer at 3306.8 cm^{-1} (−4.7 cm^{-1}) and the doubly degenerate infrared active mode at 3273.6 cm^{-1} (−37.9 cm^{-1}) for the cyclic trimer.[6] In our low-resolution spectrum the close coincidence of the free C–H stretching frequencies in the linear dimer and trimer results in a single weak feature which appears at 3307.8 cm^{-1} (−3.7 cm^{-1}) between the monomer P(1) and P(2) lines in Figure 1A. The cyclic trimer feature appears prominently in Figure 1A and is labeled Δ.

Moving to lower frequency from the bound $(HCN)_2$ feature four bands appear at 3231.0 cm^{-1} (−80.5 cm^{-1}), 3212.5 cm^{-1} (−99.0 cm^{-1}), 3201.7 cm^{-1} (−109.8 cm^{-1}), and 3182.5 cm^{-1} (−129.0 cm^{-1}) which are labeled d_1, T, d_2, and d_3 in Figure 1A. The rotationally resolved high-resolution spectrum of the 3212.5 cm^{-1} (−99.0 cm^{-1}) feature presented in Figure 3 shows that it arises from the linear trimer of HCN. The missing Q branch and evenly spaced P and R branch transitions indicate that this is a $\Sigma^+ \leftarrow \Sigma^+$ transition in a linear molecule. The measured line spacing gives a B value of 470 ± 20 MHz in agreement with previously measured spectra of the linear trimer.[6] The three features d_1, d_2, and d_3 do not have resolvable rotational fine structure and remain unassigned. None is due solely to the third band expected for the linear trimer since all three increase in intensity more rapidly than the known linear trimer features as the stagnation pressure is increased as shown in Figure 1A–C. The pressure dependence of the intensity of these bands suggests that these three feature may be due to tetramers and higher order clusters and increase in size going from d_1 to d_2 to d_3. Alternatively, they may arise from different trimer isomers whose relative concentrations depend on the expansion conditions.

Prominent groups of four and five features red-shifted from d_3 can be found in Figure 1, B and C, and may be associated with higher polymers. These and other transitions which we identify as polymer P cannot now be given unique assignments. The gas-phase CARS spectra of jet-cooled $(HCN)_n$ are consistent with these polymer features.[4] In the CARS study a broad feature (50 cm^{-1}) near 3160 cm^{-1} (−152 cm^{-1}) assigned to trimers and higher polymers spans the region we have associated with polymer transitions.

In Figure 2A the diffuse feature, S, at 3130.5 cm^{-1} (−181.0 cm^{-1}) coincides with the low-temperature (II) phase of bulk crystalline HCN.[27] The vertical dashed line at 3130 cm^{-1} marks the peak frequency of the absorption spectrum of bulk crystalline HCN(II) and the horizontal bar indicates its width at half-intensity.[27] Although the frequency of this cluster feature is identical with the peak of the bulk spectrum, the 10-cm^{-1} width of the solidlike cluster is substantially narrower than the 61-cm^{-1} width obtained from the infrared study of bulk crystalline HCN(II). Both line shapes are similar, trailing off to the high-frequency side. The small feature on the low-frequency side, shifted about $-10\ \mathrm{cm}^{-1}$ from the cluster peak, is not observed in the bulk infrared study. This feature may be due to crystal defects frozen in during formation of the clusters, or due to absorption by molecules on the faces of the small crystallites in the beam.

In a 5% mixture expanded at 450 kPa, the observed broad peak in Figure 2B contains no hint of the low-temperature phase. We suggest that this band be associated with the high-temperature solid phase of HCN or with an amorphous cluster. For reference, the location and width of the HCN(I) bulk absorption spectrum are indicated by the vertical dashed line and horizontal bar in Figure 2B.[27] The peak of the cluster spectrum is at $3159\ \mathrm{cm}^{-1}$ ($-153\ \mathrm{cm}^{-1}$) compared to a frequency of $3145\ \mathrm{cm}^{-1}$ ($-167\ \mathrm{cm}^{-1}$) for the higher temperature crystalline (I) phase of the solid. The $30\text{-}\mathrm{cm}^{-1}$ width of the cluster spectrum is again narrower than the $72\text{-}\mathrm{cm}^{-1}$ width from the infrared study of bulk crystalline HCN(I). The absence of the $3130.5\text{-}\mathrm{cm}^{-1}$ ($-181.0\text{-}\mathrm{cm}^{-1}$) band in Figure 2B suggests that for this spectrum the cluster temperature is greater than 170 K, the temperature of the I–II phase transition. The heat released on polymerization, rather than being carried away by third-body collisions or by evaporation of surface molecules, has thus been trapped within the cluster to raise its temperature.

Also indicated in Figure 2A are the position and width of the infrared absorption spectrum of liquid HCN.[27] The peak frequency appears at $3206\ \mathrm{cm}^{-1}$ for the liquid at −5 °C. This frequency is within $7\ \mathrm{cm}^{-1}$ of the observed linear trimer bound C–H stretching frequency. This near match is understood if the nature of liquid HCN is considered. The dielectric constant of the liquid is approximately 3 times that predicted from a simple model relating dielectric constant to dipole moment of monomeric HCN. On this basis Pauling[9] concluded that the average degree of association in the liquid is three; that is, the liquid consists of linear trimeric units. It is therefore reasonable that the observed linear trimer bound frequency resembles that of the bulk liquid.

Several infrared studies of matrix-isolated HCN aggregates have been completed[22-26] and may be compared to our results. The clearest investigation of the dimer in an Ar matrix shows the free C–H stretching frequency at $3306\ \mathrm{cm}^{-1}$ ($-6\ \mathrm{cm}^{-1}$) and the bound C–H stretching frequency at $3213\ \mathrm{cm}^{-1}$ ($-99\ \mathrm{cm}^{-1}$). In this study, the photolysis of matrix isolated *s*-tetrazine quantitatively produces $(HCN)_2$ and N_2.[24] For the codeposited HCN:Ar matrix the two shifts are −8.9 and $-109.4\ \mathrm{cm}^{-1}$.[22] Our molecular beam dimer shifts are −3.5 and $-70.2\ \mathrm{cm}^{-1}$. It should be noted that shifts due to the matrix environments can be large. For example, the monomer C–H vibration is shifted from the gas-phase C–H frequency by −16.8, −7.6, and $-20.3\ \mathrm{cm}^{-1}$ in Ne, Ar, and Kr matrices, respectively. For the free C–H vibration of polymers in the Ar matrix, the total shift remains small. The dimer, trimer, and tetramer shifts are −8.9, −15.0, and $-20.1\ \mathrm{cm}^{-1}$. By contrast, we find smaller shifts for the free C–H stretching vibration in the molecular beam study. For the dimer and trimer the shifts are −3.5 and $-4.7\ \mathrm{cm}^{-1}$,[6] with the linear tetramer free C–H remaining unobserved. The two bonded C–H stretching trimer features appear at shifts[22] of −114 and $-131\ \mathrm{cm}^{-1}$ compared to our low-frequency trimer shift of $-99.0\ \mathrm{cm}^{-1}$. In the matrix, higher order polymer shifts (excluding the free C–H vibration) occur in the range −125 to $-188\ \mathrm{cm}^{-1}$.[22] Our results show higher order peaks at −80.5, −109.8, $-129.0\ \mathrm{cm}^{-1}$, and in the range −141 to $-172\ \mathrm{cm}^{-1}$ with the diffuse band at $-181.0\ \mathrm{cm}^{-1}$ associated with the low-temperature solid phase of hydrogen cyanide. The matrix results agree generally with our study. Discrepancies can be attributed to additional shifts due to the matrix.

B. Modeling the Vibrational Frequencies. The vibrational energy shifts for HCN after complexation were modeled for several reasons. First, this system is ideal for testing theories of shifts due to hydrogen bonding in small complexes of known geometry. For example, a model that correctly produces the shift for the linear dimer can then be tested on higher aggregates, progressing toward the solid. Second, a reliable model for the shifts due to hydrogen bonding would allow the identification of higher complexes. Additionally, the assignment of features to specific C–H vibrational modes within a complex of a certain size would be possible.

1. Normal-Mode Analysis. The first simple approach to the modeling of the system was through normal-mode analysis. Although this method was not successful in predicting shifts in vibrational frequency due to hydrogen bonding it was useful for understanding the form of the normal modes of the clusters. Normal-mode analysis has been applied to other $(HCN)_n$ systems.[4,22]

In modeling the normal-mode stretching frequencies of the clusters, we used force fields similar to those suggested by Maroncelli et al.[4]. That is, each HCN unit in the cluster is represented by $f_{\mathrm{CH,CH}}$, $f_{\mathrm{CN,CN}}$, and $f_{\mathrm{CH,CN}}$ force constants obtained from the observed frequencies of HCN and DCN. Two monomers were then coupled with the intermolecular force constant f_s from the microwave study.[4] A normal-coordinate analysis using a standard program[36] was then performed. In contrast to previous treatments, we have not reoptimized any force constants on complexation so that we may test the sensitivity of the analysis to the choice of force constants.

The free C–H frequency for the dimer was unshifted from the monomer frequency. This is in basic agreement with our experiments which find a small, $-3.5\ \mathrm{cm}^{-1}$, shift. The bound C–H frequency is calculated to shift to the blue by $+24\ \mathrm{cm}^{-1}$. This shift can be understood by using the harmonic oscillator expression

$$\tilde{\nu}'/\tilde{\nu} = (f'/f)^{1/2} \tag{1}$$

relating a change in frequency $\tilde{\nu}$ to a change in force constant f. A shift of $+29\ \mathrm{cm}^{-1}$ is predicted if the effective force constant for the bound C–H is taken to be

$$f' = f_{\mathrm{CH,CH}} + f_s \tag{2}$$

with $f = f_{\mathrm{CH,CH}}$ and $\tilde{\nu} = 3312\ \mathrm{cm}^{-1}$, the monomer C–H frequency. Since the $+24\text{-}\mathrm{cm}^{-1}$ shift from the normal-coordinate analysis is similar to the $+29\text{-}\mathrm{cm}^{-1}$ shift predicted by the simple force constant considerations, the "coupling" effect of dimer formation, aside from the trivial increase in effective force constant, is negligible compared to the magnitude of the observed shift which is $-70.2\ \mathrm{cm}^{-1}$. Clearly a significant reduction in the bonded $f_{\mathrm{CH,CH}}$ force constant is required to fit this shift.

Each observed C–H stretching frequency may be reproduced by a simple variation of the corresponding $f_{\mathrm{CH,CH}}$ force constant. As a result, normal-mode analysis has limited power in predicting C–H frequency shifts as a function of cluster size. For example, we optimized the two $f_{\mathrm{CH,CH}}$ force constants to reflect the observed dimer frequencies and then used them in the trimer (free $f_{\mathrm{CH,CH}}$ for the free C–H and bound $f_{\mathrm{CH,CH}}$ for the other two). The calculated trimer frequencies are essentially coincident with those of the dimer in disagreement with the data. The frequency of the free C–H falls at the free C–H stretching frequency for the dimer and the other two fell at the bound C–H stretching frequency of the dimer.

A similar failure of normal-coordinate analysis in predicting the frequencies for the higher polymers and for the solid is expected. From the spread in polymer frequencies, we conclude that each polymer would require its own set of C–H stretching force constants.

The nature of the motion of each normal mode can be determined from the potential energy distribution.[37] This distribution reflects the contribution of each internal coordinate to the total change in potential energy as the molecule is distorted along a particular normal coordinate. From this analysis each of the two C–H stretching vibrational modes in the dimer consist of uncoupled C–H motions, further illustrating the independent nature of the C–H stretching vibrations. The uncoupled C–H vibrations mean that the calculated normal-mode frequency is a reflection

---

(36) Peterson, M.; McIntosh, D. *QCPE* Program No. QCMP 012.

(37) Levin, I. W.; Pearce, R. A. R. *Intramolecular Force Field Calculations: Methods and Applications in Vibrational Spectra and Structure*, Durig, J. R., Ed.; Elsevier: New York, 1975; Vol 4, Chapter 3.

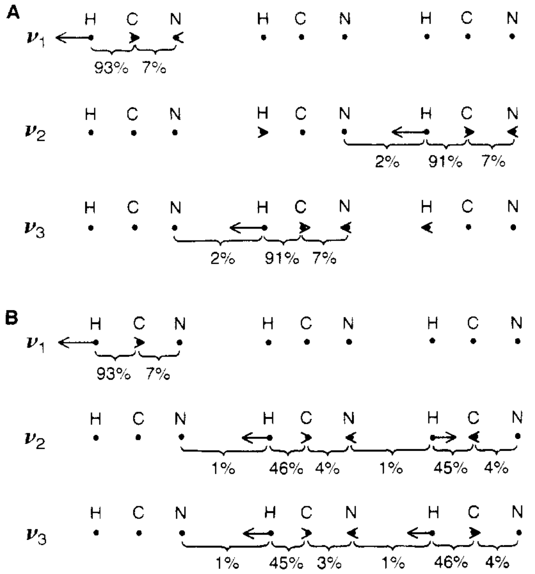

Figure 4. Normal modes for linear $(HCN)_3$. The length of an arrow is proportional to the Cartesian displacement of the atom. The percentages indicate the contribution of a particular internal coordinate to the potential energy distribution. In (A) the frequencies correspond to a fit to observed trimer frequencies (see text for details). In (B) a resonance effect is demonstrated when two C–H stretching force constants are arbitrarily equated.

of a particular $f_{\mathrm{CH,CH}}$ force constant with little connection to the rest of the molecule.

In order to picture the nature of the normal modes in the trimer we used our two molecular beam C–H stretching frequencies (Table I). We have taken the experimentally unobserved frequency to be 3225 cm^{-1} (-87 cm^{-1}) which is the value predicted by the ab initio calculations discussed below.[7] Figure 4A shows the normal modes for the trimer obtained from the force field described above ($f_{\mathrm{CH,CH}}$, $f_{\mathrm{CN,CN}}$, and $f_{\mathrm{CH,CN}}$ for each HCN unit, plus two f_s for the intermolecular stretching force constants), with the three $f_{\mathrm{CH,CH}}$ force constants fit to the two observed trimer frequencies and one ab initio calculated frequency. As can be seen from Figure 4A, each normal mode is essentially an independent C–H motion. The length of each arrow is proportional to the Cartesian displacement of the atom when the molecule is stretched along a normal coordinate. The percentages indicate the contribution of each internal coordinate in the potential energy distribution.

We must not be deceived by the success in reproducing the three C–H frequencies. The success was assured by fitting *three* $f_{\mathrm{CH,CH}}$ force constants to *three* C–H frequencies. Except for its simplicity there is nothing unique about the force constant matrix we choose. Other matrices with on- and off-diagonal terms could equally well be fit to the observed frequencies. Moreover, we have forced anharmonic motions into a collection of quadratic displacements. The apparently decoupled motions in Figure 4A may not be a realistic description of $(HCN)_3$. Let us explore our force constant field further.

As we shall see below, the actual form of the C–H motions will be important for the electrostatic modeling of the trimer and higher clusters. By changing the force constants and observing the normal modes we can test the sensitivity of the form of the normal modes to the choice of force constants. In Figure 4B the normal modes resulting from artbirarily equating the $f_{\mathrm{CH,CH}}$ for the central and bound terminal HCN units are shown. This illustrates a resonance effect that changes the two independent C–H motions into a collective motion due to the coupling provided by f_s. The form of these normal modes is sensitive to a small change in one of the two equal force constants. If one of the pair is increased by 0.1% then the C–H oscillators begin to decouple. The ratio of the contributions of the C–H internal coordinates to the normal modes becomes 72:18 as opposed to 46:45 for Figure 4B, as determined by the potential energy distribution. This ratio changes to 83:8 when the force constants differ by 0.2%. As we shall see from the force constant field generated from our ab initio calculations, the description of the normal-mode displacement is closer to Figure 4B than Figure 4A. The C–H displacements are coupled.

The form of the normal mode is also important in determining its infrared intensity. In comparing ν_3 in Figure 4B with ν_2 one would expect ν_3 to be much more intense. In the ν_3 vibration the change in dipole moment of the two vibrating units are in phase and add constructively in contrast to the ν_2 vibration in which the out of phase motion tends to cancel the change in dipole moment during the vibration. This difference in intensity may explain why the third trimer C–H stretching frequency has not been detected.

The normal-mode analysis has been useful for picturing the vibrations in the HCN clusters. The C–H motions in the solid are certainly collective, leading to the observed diffuse band. One can be fairly certain that the C–H motions in the dimer are independent from the normal-mode analysis based on the well-separated observed C–H frequencies from the dimer. At what cluster size the normal modes become a significant admixture of C–H motions is less clear. The normal-mode analysis as described here produces C–H motions that are still independent in the trimer in conflict with the ab initio results described later. For the linear tetramer one would suspect that the C–H stretching motions of the two internal HCN molecules are mixed because the force constants are similar due to the similarity in environment. The predictive power for determining C–H stretching frequencies is limited, however, by the requirement of a different set of $f_{\mathrm{CH,CH}}$ force constants for each cluster size.

2. Electrostatic Model. A second approach to calculating the vibrational energy shifts uses the electrostatic theory developed by Liu and Dykstra.[32] In this model, the intramolecular stretching potential of one member of a cluster is influenced by electrostatic interactions with the other molecules. This is a natural approach since the shifts in vibrational frequency are dominated by a change in stretching potential, as demonstrated above for the normal-coordinate analysis. In the electrostatic picture applied to HCN polymers an additional interaction potential that is linear in the C–H stretching vibrational coordinate is added to the C–H stretching potential of the isolated molecule. This additional potential is due to electrostatic interactions between HCN molecules in the cluster. It has been shown that the linear approximation to the electrostatic interaction energy is valid for a variety of hydrogen-bonded dimers containing HF.[32] The resulting shift can be calculated by using first-order perturbation theory. Following Liu and Dykstra,[32] in the linear approximation, the interaction energy can be written

$$V^{\mathrm{int}}(r) = sr \tag{3}$$

where s is the slope of the interaction potential and r represents the intramolecular stretching coordinate. This slope is usually negative for a positive C–H displacement in HCN, meaning the electrostatic energy typically becomes more negative (more stable) upon stretching the C–H bond. For example, the HCN dipole moment increases as the H is extended from the CN. As a result an attractive dipole–dipole interaction becomes more attractive. A negative slope of the interaction potential results in a red shift. Physically this corresponds to a lengthening of the equilibrium C–H distance. For an anharmonic potential describing the isolated molecule, this lengthening results in the effective potential for the C–H vibrational displacements yielding a smaller curvature at the new equilibrium position and more closely spaced vibrational levels than in the isolated molecule. The slopes of the electrostatic properties cannot in general be determined a priori and the electrostatic properties may increase or decrease upon stretching. In addition, the slope depends on geometry and while usually negative can sometimes be positive depending on the orientation of the monomers within the cluster. For the HCN system small blue shifts were calculated for the C–H stretching frequency in some cluster geometries.

Using the interaction potential as a perturbation to the isolated molecule, the energy correction of the nth vibrational level to first order is[32]

$$H'_{nn} = s\langle r\rangle_{nn} \tag{4}$$

where the matrix element involves isolated molecule wave functions. From this, the first-order shift in the transition frequency is[32]

$$\Delta\tilde{\nu}_{mn} = s(\langle r\rangle_{mm} - \langle r\rangle_{nn}) \tag{5}$$

We shall be seeking the shift of the fundamental transition, $\Delta\tilde{\nu}_{10}$. A simplifying feature of this model is that properties of the complex may be calculated from properties of the isolated molecule.

We have applied the model of Liu and Dykstra to the $(HCN)_n$ system. Briefly, the electrostatic constants that were considered are $\boldsymbol{\mu}$, $\mathbf{Q}$, and $\mathbf{R}$, which represent the tensors of the first, second, and third moments of charge (related to the dipole, quadrupole ($\boldsymbol{\theta}$), and octopole ($\boldsymbol{\phi}$) moments) and the dipole and quadrupole polarizabilities and hyperpolarizabilities represented by the tensors $\boldsymbol{\alpha}$, $\boldsymbol{\beta}$, $\mathbf{A}$, $\mathbf{B}$, and $\mathbf{C}$.[42] Interactions were considered that involve the first three nonzero permanent moments, plus induced first (dipole) and second (quadrupole) moments. In calculating the interaction energy the polymer geometry was first specified. Each molecule was then polarized by the fields due to the total moments (permanent plus induced) of all the other molecules in the cluster. By iterating this process, a self-consistent set of fields, field gradients, and higher derivatives of the electrostatic potential were obtained along with the total moments. The interaction energy was then calculated by considering the total moments of each molecule in the final field due to the other molecules plus the energy required to polarize each molecule at the final field value. With the intermolecular cluster geometry frozen the interaction energy was again calculated, but with one molecule of the cluster distorted along the intramolecular coordinate for the C–H stretching vibration. This calculation was repeated for several small distortions near the equilibrium intramolecular geometry for this molecule in the cluster while the others remained in their equilibrium geometry. The slope of the interaction potential was then obtained by taking differences. That is

$$s = \Delta V^{\text{int}}/\Delta r \tag{6}$$

where ΔV^{int} is the change in interaction potential for two values of the stretching coordinate differing by Δr.

Several pieces of information must be supplied in order to begin this calculation. First, the cluster geometry must be provided. Since there is no minimum in the electrostatic energy, some structural constraints must be obtained from other sources. Microwave spectroscopy has been used to determine the geometry of the dimer[1] and trimer,[38] providing intermolecular separation and orientation. The crystal structure has been determined for both solid phases using X-ray diffraction.[10] Van der Waals radii[39] and their analogues for hydrogen bonds[40] provide a guide for other geometries. Second, the electrostatic properties must be provided. Several complications may arise here. Typical hydrogen bond lengths are shorter than the sum of van der Waals radii. At the close monomer separations within hydrogen-bonded clusters the multipole expansions used in the electrostatic model may converge slowly. As a result higher moments are important. Also, in these systems induced moments play an important role. In short, a fairly extensive set of electrostatic properties is required to complete the electrostatic treatment. Additionally, these properties are needed at equilibrium and for at least one near-equilibrium value of the C–H stretching coordinate. Finally, the electrostatic properties must be calculated with care. This has been discussed elsewhere.[32,41] The electrostatic properties (evaluated about the center of mass) used in this study were calculated by Dykstra and Liu[31,41] using the derivative Hartree–Fock approach and correlated wave functions.[32,41] The matrix elements in eq 5, $\langle r\rangle_{11}$ and $\langle r\rangle_{00}$, were also obtained from Liu and Dykstra.[31]

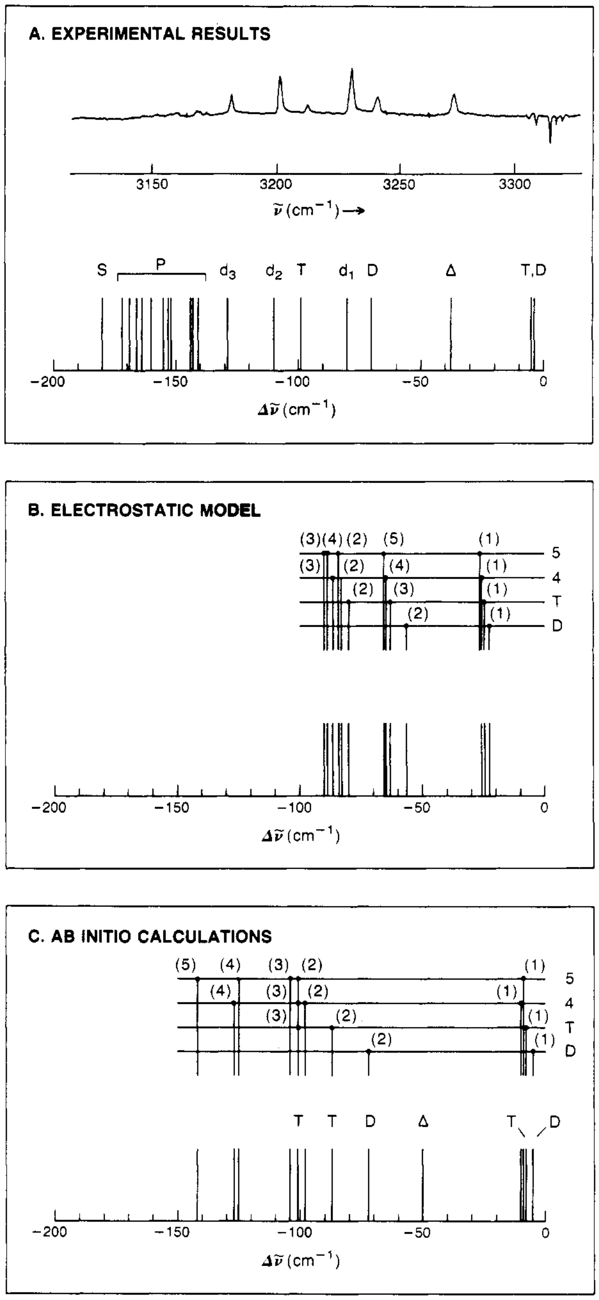

Figure 5. A comparison of electrostatic modeling (B) and ab initio calculations (C) with experimentally determined vibrational frequency shifts (A) for HCN clusters. The top half of (A) is a reproduction of Figure 1A. The bottom half is a composite stick spectrum showing the position of all observed $(HCN)_n$ features. The labeling is the same as in Figures 1 and 2. In parts B and C, D, T, 4, and 5 identify linear dimer, linear trimer, linear tetramer, and linear pentamer.

Our results are summarized in Figure 5. In Figure 5A the experimental results are reproduced in a stick spectrum, with the spectrum from Figure 1A reproduced above it for reference. Figure 5B shows the shifts calculated by using the electrostatic model for the linear dimer (D), trimer (T), and tetramer (4) with the center of mass separation of 4.45 Å, taken from the zero point averaged center of mass distance for the dimer[1] used for all the polymers. The molecular units within a chain are numbered starting from the free (non-hydrogen-bonded C–H) end of the chain. If the trimer separations are slightly contracted, as indicated

---

(38) Ruoff, R. S.; Emilsson, T.; Klots, T. D.; Chuang, C.; Gutowsky, H. S. Paper presented, at the 41st Symposium on Molecular Spectroscopy, Ohio State University, June 16–20, 1986; TF13. Ruoff, R. S.; Klots, T.; Chuang, C.; Emilsson, T.; Gutowsky, H. S. *J. Chem. Phys.*, in press.

(39) Bondi, A. *J. Phys. Chem.* **1964**, *68*, 441.

(40) Liu, S.-Y.; Dykstra, C. E. *Chem. Phys.* **1986**, *107*, 343.

(41) Dykstra, C. E.; Liu, S.-Y.; Malik, D. J. *Adv. Chem. Phys.*, in press.

(42) Applequist, J. *Chem. Phys.* **1984**, *85*, 279 and references therein.

by the microwave study,[38] to R_{12} = 4.41 Å and R_{23} = 4.37 Å then there are additional shifts of −1, −4, and −5 cm^{-1} for T(1), T(2), and T(3), respectively. A pattern is seen developing for the linear polymer within this model. For the dimer, the free, D(1), and bound, D(2), C–H frequencies are shifted −22.4 and −56.6 cm^{-1}. In going to the trimer, the free end, T(1), is only slightly shifted from D(1) to −24.7 cm^{-1}. Similarly, T(3), the bound terminal end of the trimer is shifted an additional −6.5 cm^{-1} to −63.1 cm^{-1}. The central unit in the trimer, T(2), is shifted −80.2 cm^{-1}, roughly the sum of the two dimer shifts. Comparing the calculated tetramer features shows the terminal C–H frequencies each shifted slightly to −25.5 and −64.9 cm^{-1} for 4(1) and 4(4). The two central C–H frequencies have shifts similar to T(2) in the trimer, specifically −83.1 cm^{-1} for 4(2) and −86.8 cm^{-1} for 4(3). In this model, the general spectrum for the linear polymer breaks into three groups of bands. One group contains the terminal free C–H stretching frequencies (D(1), T(1), 4(1), etc.) with small red shifts from monomer HCN. The second group contains the terminal bonded C–H stretch frequencies (D(2), T(3), 4(4), etc.) and third there are the interior (nonterminal) C–H frequencies which display the largest red shift. The calculated frequencies for longer linear polymers continue to fall in these groups. This demarcation has been suggested in other spectroscopic studies for the matrix-isolated $(HCN)_n$[25,26] but is not supported by our molecular beams study since there is no evidence that we have observed any linear complex longer than trimer. Comparison of the electrostatic model to our results is therefore limited to the two linear dimer frequencies and the two observed linear trimer frequencies. For the bound C–H stretching frequency in the dimer the model prediction differs from the observed shift by 18.9 cm^{-1}. The prediction of −22.4 cm^{-1} for the free C–H stretching frequency shift is in disagreement with the observed −3.5-cm^{-1} shift. The magnitude of the decrease in stretching frequency of the free C–H in going from the dimer to trimer is correctly modeled yet the absolute shift for the free C–H stretching vibration in the linear trimer at −24.7 cm^{-1} also disagrees with the observed −4.7-cm^{-1} shift. None of the other predicted shifts for the linear trimer agree well with the observed band at a shift of −99.0 cm^{-1}, with the largest predicted trimer shift falling at −80.2 cm^{-1}. Although the bound dimer C–H frequency shift agrees well with that predicted by the electrostatic model, there is substantial disagreement in the other comparisons.

In order to understand the source of disagreement for the linear dimer and trimer, simple changes in the center of mass separations in the linear polymer were considered. For example, a previous calculation for the HCN dimer shifts used a separation of 4.209 Å.[31] This corresponds to the equilibrium, as opposed to the zero point averaged, separation as predicted by the hydrogen bond analogues of van der Waals radii. These were obtained by ab initio methods and tested against experimentally determined equilibrium bond lengths where available.[40] The effect of this shortening is to further red shift the spectrum from the monomer due to a stronger electrostatic interaction at the shorter hydrogen bond length. The frequencies at the shorter separation appear at −30.5 and −75.9 cm^{-1}. Thus, while the bound C–H frequency comes into closer agreement with the observed result the free C–H frequency becomes more disparate. Increasing the center of mass separation to better fit the free C–H stretching frequency shift in the dimer resulted in a poorer fit of the bound C–H stretching frequency shift. Adjustments of center of mass separations for the trimer likewise cannot reconcile all the electrostatic predictions with the data.

As a final test the vibrational energy shift of the solid was predicted by using the electrostatic model. A large cluster of HCN molecules was constructed with the individual molecules placed at the crystal lattice positions and orientation for the low-temperature solid phase as determined by X-ray diffraction.[10] The frequency shift of the central molecule was calculated. For a cluster size of 135 molecules, which includes all HCN molecules in a cylindrical volume 26.04 Å (7 molecules) long with a 7.7-Å radius, the shift of the central HCN was −60.5 cm^{-1}, one-third of the shift of the diffuse feature at −181.0 cm^{-1} in the present study and the coinciding shift of solid HCN.[27] This calculated shift is roughly three-fourths of the electrostatic prediction for the central units of the linear trimer or tetramer. The difference between the central molecules in the linear polymer and the solid is due to the interaction with the off-axis HCN molecules in the solid. Changing the positions of the molecules in the $(HCN)_{135}$ cluster to correspond to the high-temperature HCN(I) phase[10] resulted in a −64.2-cm^{-1} shift, in poor agreement with the observed −167-cm^{-1} shift.[27]

The electrostatic model has not reproduced the observed shifts for the linear dimer and trimer nor the shift in the solid, for which the geometry is known from the X-ray diffraction study.

3. Ab Initio Calculations. Since the simpler treatments have not been sufficient to describe the vibrational energy shifts of the HCN clusters, we now turn to the more complete ab initio methods. First we will consider SCF calculations done elsewhere[7] and then will present our own results both at the SCF level and with electron correlation included.

The harmonic vibrational frequencies were recently calculated by Kofranek, Karpfen, and Lischka at the SCF level for $(HCN)_n$ clusters for n = 1–5.[7] The results from this study for the linear polymers are summarized in Figure 5C. The vibrational frequencies in the dimer (D), trimer (T), tetramer (4), and pentamer (5) are numbered starting from the highest frequency mode. The frequency shifts in this figure have been derived from calculated frequencies that have been scaled in the original calculation. The scaling factor is the ratio of the observed monomer (anharmonic) frequency to the calculated monomer (harmonic) frequency. The same factor was used for all calculated frequencies. The frequency shifts corresponding to the scaled results are about 10% smaller than those unscaled.

Comparison of the frequency shifts of all assigned bands in the $(HCN)_n$ spectrum with the SCF shifts shows good agreement. Figure 5 shows this agreement between the observed small shifts for the free C–H stretching vibrations in the linear dimer and trimer and those calculated by the SCF method. The bound C–H dimer frequency shift is −70.2 cm^{-1} compared to a calculated −72-cm^{-1} shift, with the one assigned trimer bound C–H stretching frequency at −99.0 cm^{-1} falling near a calculated shift of −101 cm^{-1} for ν_3 in the linear trimer. The other bound C–H stretching mode, ν_2, has a calculated shift of −87 cm^{-1}, placing it near the diffuse d_1 band at a −80.5-cm^{-1} shift. The intensity of band d_1 does not have the same pressure dependence as the assigned 3212.5 cm^{-1} (−99.0 cm^{-1}) trimer band, so it cannot be solely due to the linear trimer. The missing trimer feature may be obscured by the d_1 band or may be sufficiently lower in intensity compared to the other two linear trimer features as to not appear in our spectrum. On the basis of the form of ν_2 calculated from a normal-mode analysis using force constants obtained from the SCF calculation, the ν_2 vibration is expected to be weaker than ν_3. This normal-mode analysis will be discussed more fully later. In reasonable agreement with the experiment is the predicted −50-cm^{-1} shift for the infrared active ν_2 in the cyclic trimer which appears at a −37-cm^{-1} shift.

The general appearance of the calculated SCF shifts can be compared to the observed spectrum and to the predictions of other models. For the free end of the chain, the frequency shift behavior is similar to the results for other models, in that the shift of this terminal C–H changes very little with chain length, starting at −5 cm^{-1} for the dimer, D(1), and increasing to −9 cm^{-1} for long chains, 5(1) for example. The lowest frequency modes show very different behavior as a function of linear polymer size. With increasing chain length the lowest frequency mode shows significant shifts. The predicted shifts are −72, −101, −127, and −142 cm^{-1} for D(2), T(3), 4(4), and 5(5). This spreading of frequencies with growing cluster size is consistent with the observed spectra, in which the features for smaller aggregates (dimer and trimer), exclusive of the free C–H stretches, appear well separated and the smaller sized polymers are spread over a 30-cm^{-1} range. Additionally, these shifts for the tetramer and pentamer are of the correct magnitude to fall in the −130- to −170-cm^{-1} region of the observed spectra, labeled P, assigned to the higher polymers.

TABLE II: Calculated Frequencies and Shifts[a]

			electrostatic model	ab initio calculation[b]		
				SCF[c]	SCF[d]	MP2[d]
HCN	ν_3	CH str		3654	3652	3536
	ν_2	HCN bend		864	881	738
	ν_3	CN str		2335	2435	2046
$(HCN)_2$	ν_1	CH str	(−22)	3648 (−6)	3647 (−5)	3533 (−3)
	ν_2	CH str	(−57)	3574 (−80)	3589 (−63)	3459 (−77)
$(HCN)_3$	ν_1	CH str	(−25)	3646 (−8)	3643 (−9)	
	ν_2	CH str	(−63)	3557 (−97)	3577 (−75)	
	ν_3	CH str	(−80)	3544 (−110)	3566 (−86)	
			Other Vibrational Modes			
$(HCN)_2$		CN str		2347	2444	2064
		CN str		2323	2426	2048
		HCN bend		965	893	738
		HCN bend		880	974	916
		CN str		122	114	129
		$(HCN)_2$ bend		158	144	161
		$(HCN)_2$ bend		54	49	56
$(HCN)_3$		CN str		2349	2445	
		CN str		2332	2432	
		CN str		2319	2423	
		HCN bend		987	896	
		HCN bend		980	995	
		HCN bend		883	986	
		$(HCN)_3$ str		165	153	
		$(HCN)_3$ str		92	85	
		$(HCN)_3$ bend		193	176	
		$(HCN)_3$ bend		142	130	
		$(HCN)_3$ bend		67	63	
		$(HCN)_3$ bend		17	17	

[a] All frequencies and shifts are in cm^{-1}. [b] These frequencies are unscaled. The cluster shifts are relative to the calculated monomer frequency. [c] Reference 7, basis set 1. [d] This work, 6-31G** basis set.

There is also a spread in predicted shifts for other modes. The shift for T(2) is -87 cm^{-1} and that for 5(4) is -125 cm^{-1}, and a collection of other modes (4(2), 4(3), 5(2), and 5(3)) fall in the region -100 ± 5 cm^{-1}. This spread in molecule vibrational frequency shifts, -87 to -125 cm^{-1}, is somewhat larger than those calculated by the electrostatic model which fall in the -85- to -97-cm^{-1} range. The magnitude of these interior molecule frequency shifts in the electrostatic model is comparable to those from the SCF calculation. Although no specific higher polymer bands have been assigned, one would expect the interior molecule frequencies to fall in the -130- to -170-cm^{-1} range. The bound trimer feature appears near one end of the range and the solidlike feature, certainly due to an interior molecule, appears near the other. A second related SCF study[30] calculates the vibrational frequency shift for an infinite HCN chain to be -137.9 cm^{-1}, or -125.3 cm^{-1} if scaled as described above. This model accounts for 70% of the observed shift for the low-temperature solid phase. This is reasonable for a model of the solid that neglects the off-axis molecules.

We have repeated the ab initio SCF calculations for the HCN monomer, linear dimer, and linear trimer using a 6-31G** basis set[64] to obtain the quadratic force constants, from which the normal-mode frequencies were calculated. These ab initio frequencies essentially agree with those in the work of Kofranek, Karpfen, and Lischka[7] which were described above. Our results have been included in Table II for comparison. We have also used our ab initio quadratic force constants to obtain the form of each normal mode through the potential energy distribution. This analysis shows the two high-frequency modes in the dimer to be independent CH stretching motions, each resembling the C–H stretching mode in the monomer. The motion of the higher frequency mode, ν_1, is confined to the acceptor HCN molecule with 96% in the C–H and 4% in the C–N stretching vibrations as determined by the potential energy distribution.[37] For the lower of the two frequencies, ν_2, the stretching motion is 94% in C–H and 2% in C–N of the donor HCN molecule with 2% in the intermolecular hydrogen bond stretching motion. The remaining motion is distributed in the other HCN molecule. These results are in close agreement with our normal-coordinate analysis.

For the trimer, our SCF results find the C–H stretching motions to be significantly different from those in the dimer for two of the C–H modes, while the third closely resembles a dimer mode. The highest frequency mode, ν_1, in the trimer consists of independent motion of the terminal acceptor HCN molecule. The potential energy distribution shows 92% C–H motion and 8% in C–N. The other two high-frequency modes, on the other hand, are an admixture of C–H motions of the central and donor terminal HCN. For ν_2, the out-of-phase admixture, the stretching motion is distributed into 32% C–H and 3% C–N of the central molecule with 58% C–H and 5% C–N stretch of the donor terminal molecule. For ν_3, the in-phase admixture, the roles are reversed with 58% C–H and 5% in C–N stretching motion in the central molecule and 32% C–H and 3% C–N in the donor terminal molecule. This distribution of motions is due to a resonance between the two HCN molecular stretches involved in the trimer normal modes. The diagonal force constants $f_{CH,CH}$ related to the stretching of the C–H internal coordinates in each of the three HCN molecules making up the trimer are 6.936, 6.709, and 6.726 mdyn/Å. If the diagonal force constant, f_s, for the intermolecular stretching vibration immediately adjacent to each C–H involved in a hydrogen bond is added to the corresponding $f_{CH,CH}$ to approximate the effective force constant for H motion, the result is the 6.836 mdyn/Å for the central HCN molecule and 6.840 mdyn/Å for the terminal donor HCN molecule. It is the near coincidence of these force constants that is responsible for the resonance. This was demonstrated in the previous normal-mode calculations by varying one of the force constants and observing the changes in the potential energy distribution. The normal modes determined in the ab initio calculation can be tested in the same way. We arbitrarily chose to vary the SCF force constant $f_{CH,CH}$ for the donor terminal HCN. The ratio of contributions of the two C–H stretching coordinates in the pair for the SCF calculated force constants is 58:32. This ratio is 72:18 when the terminal donor C–H force constant is increased by 0.3% and changes to 80:10 when the force constant is increased by 0.6%. The two pertinent frequencies for the SCF calculated force constants are separated by 11.3 cm^{-1}. For the changed force constant (producing the 80:10 ratio) the frequency separation is 18.8 cm^{-1}. Since the splitting of frequency between the two bound C–H stretching modes is not known, the admixture of the C–H motions making up each normal mode cannot be determined, except through the ab initio calculations.

As was pointed out earlier, the form of the molecular vibration must be borne in mind when applying the electrostatic model, which assumes that each C–H vibration is an independent motion. It appears that this assumption is valid for the dimer and for the free end of the trimer on the basis of the SCF calculation and on the normal-mode analysis of the observed frequencies. The results for the other two modes in the trimer are inconclusive. Based on the simple normal-mode analysis of the two observed linear trimer frequencies the other two modes are independent as illustrated in Figure 4A. The normal modes based on force constants from the ab initio calculation do not support this conclusion, although the predicted frequency splitting may exaggerate the collective nature of the modes.

In order to include electron correlation effects, which are absent from the SCF calculations, we have completed a second-order Møller–Plesset perturbation (MP2) calculation for the HCN monomer and dimer using the 6-31G** basis set.[64] The normal-mode frequencies determined at this level of calculation have been included in Table II. Considering first the monomer, there is significant improvement in the agreement with the experimentally determined harmonic frequencies, although the calculated C–H stretching frequency is still too high by 94 cm^{-1}. A similar improvement in absolute frequency is seen for the dimer normal-mode frequencies. The calculated shifts relative to the MP2 monomer C–H frequency, however, are similar to the shifts obtained from the SCF calculations. The inclusion of electron correlation effects does not appreciably affect the predicted shifts although the absolute frequency is improved.

Recently an MP2 calculation has been completed on a related system, HCN···HF, by Amos et al.[43] A correlation contribution of -49 cm^{-1} for the monomer to complex harmonic frequency shift for HF brought the calculated shift to -238 cm^{-1} from -189 cm^{-1} at the SCF level compared to the observed shift at -245.2 cm^{-1}.[43] For the vibrations involving HCN, the correlation contributions to the shifts are smaller, $+5$ cm^{-1} for the C–H stretch, $+14$ cm^{-1} for the C–N stretch, and -9 cm^{-1} for the HCN bend. The observed shift for the C–H stretching frequency is only -1.14 cm^{-1}.[65] Our MP2 results for $(\text{HCN})_2$ are similar in that the correlation effects on the harmonic shifts for HCN are small.

The ab initio calculations have been adequate for the observed shifts for the linear dimer and trimer and for the cyclic trimer. The general appearance of the collection of shifts for the linear complexes when compared to the observed spectrum suggests that for the higher polymers the geometry is not simply linear. From SCF calculations comparing cyclic and linear trimer and tetramers one concludes that cyclic structures should be considered for higher polymers. In addition the observed appearance of the solidlike feature and the nearby higher polymer (P) features suggests that complexes composed of parallel linear chains should also be considered.

4. A Critique of the Models. Each of the models discussed above is successful for reproducing certain aspects of the observed spectra involving HCN clusters, but none provides a comprehensive picture of the evolution of vibrational energy shifts as the aggregates grow from the dimer to large clusters. Several shortcomings of the models should be mentioned.

All models discussed have ignored anharmonic effects. (Although the electrostatic model relies on anharmonicity in the C–H stretching vibration, other anharmonicities are ignored.) Once the harmonic approximation is left, the frequency of a mode depends not only on the zero-order (harmonic) frequency ω_i and its anharmonicity χ_{ii} but also on anharmonicities χ_{ik} related to all the other vibrational modes. This dependence is illustrated by the expression for the fundamental frequency $\tilde{\nu}_i$ of a nondegenerate vibrational mode

$$\tilde{\nu}_i = \omega_i + 2\chi_{ii} + \tfrac{1}{2}\sum_{\substack{k \\ k\neq i}} \chi_{ik} d_k \tag{7}$$

where d_k is the degeneracy of mode k.[44] The harmonic frequency ω_i depends only on the quadratic terms in the vibrational potential, whereas the χ_{ik} also depend on higher order terms. The effect of complex formation on the anharmonicities and the resulting change in vibrational frequency may come from two sources. First, anharmonicities in the complex that correlate to monomer motions may change from their corresponding values in the monomer. A second related effect is the addition of the new vibrational modes due to complexation. The effect of these is described by new terms in the sum in eq 7 above. The terms related to the low-frequency intermolecular modes may be important since these modes are potentially quite anharmonic. A recent ab initio study of hydrogen bonding involving HF and HCl demonstrated that anharmonic effects are significant, although cancellation of large effects made the overall anharmonic correction small.[43] For example, in HCN···HF the HF anharmonicity constant χ_{11} changed from -89 cm^{-1} in the monomer to -110.76 in the complex. This change was partially offset by a large (45.2 cm^{-1}) additional anharmonic constant χ_{16} related to the HF stretching motion and one of the intermolecular bends. Comparing the anharmonic contribution to the monomer HF frequency to the total anharmonic contribution to the complex HF frequency results in an overall change of $+12$ cm^{-1}.

In a related area, the three models discussed have ignored any perturbation of the vibrational energy levels due to accidental degeneracy of excited states of different vibrational modes. Actually, the possibilities for Fermi resonances are very great. For the dimer, our SCF calculations give 114 cm^{-1} for the stretching vibration, and doubly degenerate vibrations 49 and 144 cm^{-1} against the hydrogen bond. These together with the intramolecular vibrations of each HCN molecule give, by direct count, a density of states (all symmetry species included) of $10^2/\text{cm}^{-1}$ near 3300 cm^{-1}. The density of states for the trimer is orders of magnitude greater. The effects of these resonances are difficult to predict. We do find anomalies in a vibration–rotation transition bandwidth of the trimer which we believe is a consequence of resonance as we shall discuss in the following section.

The success of the electrostatic picture for bond energies was attributed to the fortuitous cancellation of other effects,[45] the most important of these being charge transfer and exchange repulsion. In a study of HCN crystal lattice energies, a calculation of the magnitude of each contribution to the total energy was made, demonstrating that the agreement of the electrostatic energy and the total hydrogen bond energy was due to almost complete cancellation of effects as large as the total energy.[46] The question arises as to the effect of these other contributions on vibrational energy shifts. For example, charge transfer may be expected to strengthen or weaken bonds inside the cluster, giving rise to shifts in the vibrational frequencies.

The electrostatic model also relies on each normal mode in a cluster being an independent C–H vibration. The normal-coordinate analysis has shown this assumption is not valid for the larger complexes, since even the modes in the trimer are mixed, as indicated by the normal modes obtained from our ab initio calculations.

Another difficulty in the electrostatic model is the determination of the correct geometry for the calculation. Certainly the electrostatic contribution to the interaction energy involves an average of the molecular position and orientations over their zero-point motions. The question is what geometry best reflects the zero point averaged geometry. This is especially difficult for weakly bound complexes that undergo large amplitude displacements. A determination of the average angular off-axis displacement for $(\text{HCN})_2$ yields 17.34° for the acceptor and 11.04° for the donor

---

(43) Amos, R. D.; Gaw, J. F.; Handy, N. C.; Simandiras, E. D.; Somasundram, K. *Theor. Chim. Acta.* **1987**, *71*, 41.

(44) Herzberg, G. *Molecular Spectra and Molecular Structure II. Infrared and Raman Spectra of Polyatomic Molecules*; Van Nostrand Reinhold: New York, 1945.

(45) Umeyama, H.; Morokuma, K. *J. Am. Chem. Soc.* **1977**, *99*, 1316.

(46) Rae, A. I. M. *Mol. Phys.* **1969**, *16*, 257.

HCN.[1] A complete vibrational averaging of electrostatic energy would be difficult. It would seem that using the zero point averaged hydrogen bond length would be an approximation to this. The success of the use of equilibrium bond lengths in conjunction with the electrostatic model has been demonstrated for a variety of hydrogen-bonded dimers.[32] The use of this bond length is hard to justify except in a semiempirical way.

As is shown in the Appendix, when certain assumptions are made regarding the nature of the vibrational motion and source of interaction between monomer units in a cluster, the electrostatic model and the ab initio harmonic calculation should agree to lowest order.

C. Vibrational Predissociation and Photoevaporation. The lifetimes for vibrational predissociation can be easily extracted from the bandwidths of the C–H stretching features. For $(HCN)_3$ we find from Figure 3 a lifetime of 3 ns for one of the bound hydrogen stretching frequencies and Miller et al.[47] determined a lifetime range for the free hydrogen of 140 ns $< \tau <$ 300 μs. These lifetime values are comparable to those reported for predissociation from the excited hydrogen stretching modes of $(HCN)_2$.[47]

A variety of theoretical treatments, some quite detailed, have been offered to calculate vibrational predissociation lifetimes.[48] These calculations become difficult as the number of degrees of freedom of the complex increases and none have been reported from hydrogen cyanide systems. We shall estimate the lifetimes using simple selection rules[49] extracted from analytical treatments of Coulson and Robertson,[50] Beswick and Jortner,[51,52] and Ewing.[53-58] In applying these selection rules the rate for vibrational predissociation is written

$$k_{\mathrm{VP}} \approx 10^{13} \exp[-\pi(\Delta n_{\mathrm{t}} + \Delta n_{\mathrm{v}} + \Delta n_{\mathrm{r}})] \qquad (8)$$

and has a simple physical explanation. The preexponential factor is related to the hydrogen-bond collision frequency which, for our case, is the frequency at which an HCN vibrates against its neighbors within $(HCN)_3$. Table II suggests that this frequency corresponds to stretching vibrations in the range $\tilde{\nu}_2 \approx 85$–153 cm^{-1}. The exponential term gives the probability that a collision will result in mixing the bound state of the vibrationally excited hydrogen-bonded complex (the initial state) with a continuum state of the predissociation fragments (the final state). This probability depends on the difference in quantum numbers between the final and initial states. The final-state translational quantum number roughly counts the number of nodes of the (near) plane wave describing the departing fragments while they are in the region of the intermolecular potential well. (It resembles the quantum number for a particle in a box, the box being defined by the size of the intermolecular potential well.) This quantum number is given by

$$q = (2\mu\Delta E)^{1/2}/a\hbar \qquad (9)$$

where μ is the reduced mass of HCN against $(HCN)_2$ within the trimer, ΔE is the translational kinetic energy of the fragments, and a is the range parameter of the Morse potential used to model the intermolecular interaction. The number of nodes of the plane wave may be correlated to the initial-state translational quantum number, v_{s}, which characterizes the stretching motion against the hydrogen bond. The effective change in translational quantum number during predissociation can be approximated by

$$\Delta n_{\mathrm{t}} \approx |q/2 - v_{\mathrm{s}}| \qquad (10)$$

Typically the probability for vibrational relaxation is reduced by an order of magnitude for each quantum number change of the chemical bond vibrational level. This leads to the relationship

$$\Delta n_{\mathrm{v}} \approx \gamma_{\mathrm{v}}|\Delta v| \qquad (11)$$

where Δv is the net change of the chemical bond vibrational quantum numbers and γ_{v}, of the order 1,[49] is a measure of the effectiveness of the coupling of the chemical bond and hydrogen bond (the bond that breaks). Finally the fragments may be produced in rotationally excited J states. Changes in the quantum numbers of rotatory origin are the most difficult to model. By analogy to the treatment of the other quantum number changes, we can write[49]

$$\Delta n_{\mathrm{r}} \approx \gamma_{\mathrm{r}}|J - v_{\mathrm{w}}| \qquad (12)$$

where v_{w} is the wagging mode quantum number of $(HCN)_3$. It is known from experimental studies of collisional relaxation of small molecules with relatively large moments of inertia that rotational relaxation plays a minor role in vibrational energy transfer.[59] Accordingly, we shall say that the proportionality constant γ_{r} is small, which is tantamount to assuming that $\Delta n_{\mathrm{r}} \approx 0$. The propensity rule expression of eq 8 states the reluctance of a vibrationally excited van der Waals molecule to predissociate when the change in the sum of all the quantum numbers (translation + rotation + vibration) is large. Thus there are stringent selection rules governing vibrational predissociation processes.

We shall proceed now to test this simple model for vibrational predissociation of $(HCN)_3$ with the bound hydrogen vibrationally excited. We look for the most efficient vibrational predissociation in that channel which suffers the smallest total quantum change:

$$(HCN)_3^* \rightarrow HCN + (HCN)_2^* + \Delta E \qquad (13)$$

Here we suggest that the departing $(HCN)_2^*$ fragment retains double excitation in the chemical bond bending modes, 1520 cm^{-1}. The energy of the double excitation was obtained by using the average bending frequency for the dimer as calculated in ref 7, scaled by the ratio of the observed monomer bending frequency to the calculated monomer bending frequency (Table II). From the SCF calculations in ref 7 the hydrogen bond energy is $D_0 \approx$ 1660 cm^{-1} and the mode excited according to our data is 3212 cm^{-1}. The net energy into translation then becomes $\Delta E = 3212 - 1660 - 1520 = 32$ cm^{-1}. A typical range parameter for a variety of complexes is 2×10^8 cm^{-1}.[49] The reduced mass for HCN departing from $(HCN)_2$ is 18 amu. Use of eq 10 reveals $\Delta n_{\mathrm{t}} \approx$ 1.5. Since $(HCN)_3^*$ suffers one vibrational quantum change and $(HCN)_2^*$ contains double bending excitation we have $\Delta n_{\mathrm{v}} = 3$. Use of eq 8 then reveals $\tau \approx 10^{-7}$ s, a discrepancy of 2 orders of magnitude from our observed 3 ns value. The simple selection rules, demonstrated to be successful for a variety of van der Waals molecules,[49] are in reasonable agreement with the experiment. Consideration of another relaxation channel to produce $(HCN)_2$ in its ground vibrational state with $\Delta n_{\mathrm{v}} = 1$ yields a larger ΔE, a greater Δn_{t}, and an even longer relaxation time.

Even this 2 orders of magnitude agreement with experiment should be considered fortuitous. The calculated hydrogen bond energy, D_{e}, from which D_0 is obtained through correction for zero point energy, varies considerably depending on the basis set used.[7] Although the most reliable D_{e} was used in the above calculation, the spread in calculated values is several hundred wavenumbers.[7] Use of other values of D_{e} results in an increase in calculated lifetime of many orders of magnitude.

This calculation of vibrational predissociation lifetime is incomplete in the sense that the role of Fermi resonance has not been included. These resonances serve to reduce the effective Δn_{t} quantum changes and have been shown in the *s*-tetrazine–Ar complex to reduce the predissociation lifetime by 5 or 6 orders of magnitude.[60] Evidence of resonance is seen in the distortion of the R(4) line of the $(HCN)_3$ ν_3 vibration shown in Figure 3.

---

(47) Jucks, K. W.; Miller, R. E. Paper presented at the 42nd Symposium on Molecular Spectroscopy, Ohio State University, June 15–19, 1987; FA8.

(48) Leroy, R. J.; Carley, J. S. *Adv. Chem. Phys.* **1980**, *42*, 353.

(49) Ewing, G. E. *J. Phys. Chem.* **1987**, *91*, 4662.

(50) Coulson, C. A.; Robertson, G. N. *Proc. R. Soc. London Ser. A* **1975**, *A342*, 289.

(51) Beswick, J. A.; Jortner, J. *Chem. Phys. Lett.* **1977**, *49*, 13.

(52) Beswick, J. A.; Jortner, J. *Adv. Chem. Phys.* **1981**, *47*, Part 1, 363.

(53) Ewing, G. E. *Chem. Phys.* **1978**, *29*, 253.

(54) Ewing, G. E. *J. Chem. Phys.* **1979**, *71*, 3143.

(55) Ewing, G. E. *Faraday Discuss. Chem. Soc.* **1982**, *73*, 325.

(56) Ewing, G. E. *Potential Energy Surfaces and Dynamics Calculations*; Truhlar, D. G., Ed.; Plenum: New York, 1981; p 75.

(57) Morales, D. A.; Ewing, G. E. *Chem. Phys.* **1980**, *53*, 163.

(58) Ewing, G. E. *J. Chem. Phys.* **1980**, *72*, 2096.

(59) Moore, C. B. *J. Chem. Phys.* **1965**, *43*, 2979.

(60) Ewing, G. E. *J. Phys. Chem.* **1986**, *90*, 1790.

Since the P(4) bandwidth is not anomalous this suggests a Fermi resonance in the $J = 5$ level of the excited vibrational state.

All HCN clusters observed in this study fragment after absorbing an infrared photon. For the small clusters this is understandable in terms of vibrational predissociation. With the larger clusters, the solidlike S feature in Figure 2A for example, this fragmentation is better understood as photoevaporation. Important for photoevaporation is the final vibrational temperature of clusters formed in the expansion, which is determined by condensation–evaporation processes during cluster formation.[61] As clusters form, the heat of condensation is carried away by a third body in a collision or goes into internal energy of the cluster. The larger the cluster, the more efficient a heat sink is provided by the internal vibrational motions of the cluster, which absorb a significant fraction of the heat of condensation and results in raising the internal temperature of the cluster. This raising of the internal energy is balanced by cooling due to evaporation of surface molecules. In the latter parts of the expansion when the collision frequency drops the evaporation dominates and cools the cluster vibrational temperature. Cooling continues until it is unlikely that another surface molecule will be ejected from the cluster. A correlation of final cluster temperature with well depth,[61] ϵ, or with heat of vaporization,[62] ΔH_{vap}, reflects this mechanism for determining the final temperature of a cluster. Clusters formed by the above scheme are in a sense on the threshold of releasing another molecule from the surface as they approach the laser–molecular beam crossing. The absorption of a photon is sufficient to raise the temperature enough to evaporate another surface molecule to again cool the cluster. It is this mechanism that is felt to be responsible for the photofragmentation of the solidlike feature in the $(HCN)_n$ spectrum.

The idea of relatively high vibrational temperatures for the larger clusters is supported by the disappearance of the S feature in going from Figure 2A to Figure 2B which suggests that the HCN(II) to HCN(I) phase transition temperature of 170 K has been exceeded. This is further supported by applying to $(HCN)_n$ the correlation of final cluster temperature, T_{cl}, with heat of vaporization, ΔH_{vap},[62]

$$T_{\text{cl}} \approx k\Delta H_{\text{vap}} \tag{14}$$

which was empirically obtained from diffraction studies of clusters formed in neat supersonic expansion of a variety of molecules. In this expression k is a constant with a value of 7.3 kJ^{-1} mol K.[62] Using the heat of vaporization at its normal boiling point[63] of 25.22 kJ mol^{-1} yields a final HCN cluster temperature of 184 K which is consistent with the temperature of the large clusters being near the phase transition with the actual temperature depending on the details of the expansion conditions. Additional cooling is expected due to the presence of the helium carrier.

Conclusion

A large number of peaks from different size clusters of HCN have been observed ranging from dimer and trimer, through higher polymers to aggregates that exhibit solidlike behavior. Spectral features associated with these clusters span about 180 cm^{-1}, being well separated for the smaller polymers and only becoming congested in the region where the higher polymers absorb. In tuning the cluster size distribution by adjusting the expansion conditions the contribution of a particular polymer to the spectrum can be enhanced. When expansion conditions favor large aggregate formation, solidlike behavior is seen with evidence of phase transitions. In the HCN system the evolution from small polymers to large clusters is complicated by the existence of cyclic structures. These may make cluster growth not simply aggregation of linear dimers and trimers into the linear hydrogen-bonded chains found in crystalline HCN. Yet the evolution in cluster size should prove important in linking the properties of hydrogen bonded clusters to those of bulk phases.

Although a wealth of information is contained in the spectroscopic studies of $(HCN)_n$ a complete modeling of the system was not possible. The normal-coordinate analysis suffers from the lack of vibrational frequencies to completely characterize the quadratic vibrational potential. However, we have shown that the dependence of the C–H stretching frequencies on the change in force constant upon complexation is more important than mechanical coupling to the rest of the cluster. This limits the predictive power of the normal-mode treatment since short of ab initio calculations we have no way of knowing how the force constants vary with degree of complexation. The qualitative description of the vibrational modes is nevertheless useful.

In the electrostatic treatment other effects that fall outside the assumptions of the simple model may be important in determining the vibrational frequency shifts. The simple model can only treat vibrational motion localized in a single monomer unit of the cluster. Our analysis shows that this localization breaks down in the larger polymers and the C–H modes become mixed. Anharmonicities, especially those related to the intermolecular motions, have been neglected. Further difficulties in the model include uncertainties in cluster geometry, and the large number of electrostatic constants required for the calculation, most of which are not readily available.

The ab initio calculations have been the most successful in calculating vibrational shifts, but still have some shortcomings. For the ab initio treatments considered, anharmonicity has again been neglected. Its inclusion may be difficult, since terms higher than quartic in the vibrational potential have been shown to be important for other hydrogen-bonded systems, HCN···HF in particular.[43] Although electron correlation has been shown to be important in the modeling of vibrational frequency shifts in HCN···HF, our MP2 calculation shows the inclusion of electron correlation does not appreciably affect the shift although the absolute frequency is improved. The absolute error in calculated vibrational frequencies for the ab initio methods is still large. For the SCF calculation the error is about 200 cm^{-1} for ν_3 in the monomer, which is reduced to 94 cm^{-1} for the MP2 calculation. These errors are as large as the shifts due to hydrogen bond formation. However, an empirically chosen constant scaling factor to correct for anharmonicity in the monomer is successful in reproducing shifts of low-order polymers.

Our understanding of the origin of vibrational energy shifts upon hydrogen bond formation in the HCN system is not complete. When new models are developed, the hydrogen cyanide system will provide a stringent test. Additionally, this system will provide an equally vigorous test for other cluster properties as a function of size. This should lead to a better understanding of molecular properties as the evolution from the gas phase to condensed phases is followed.

Acknowledgment. Discussions with James Reilly throughout this study have been particularly useful. The support of the National Science Foundation is gratefully acknowledged.

Appendix

At first glance the electrostatic model of Liu and Dykstra[32] and the ab initio harmonic oscillator model seem contradictory because the electrostatic model relies explicitly on the change in the average value of the coordinate upon vibrational excitation. This change comes entirely from anharmonicity in the vibrational potential. The ab initio model determines vibrational frequencies by evaluating harmonic force constants at the minimum of the calculated vibrational potential. Under certain assumptions, however, the electrostatic model is equivalent, in lowest order perturbation theory, to the harmonic oscillator model. It is important to understand these assumptions since, when they are not valid, the electrostatic model is likely to produce incorrect results.

Consider first a general perturbation treatment and the assumptions necessary for agreement between the electrostatic model and the ab initio calculation. The first assumption is that localized

---

(61) Farges, J.; de Feraudy, M. F.; Raoult, B.; Torchet, G. *Surf. Sci.* **1981**, *106*, 95.

(62) Valente, E. J.; Bartell, L. S. *J. Chem. Phys.* **1984**, *80*, 1451.

(63) Giauque, W. F.; Ruehrwein, R. A. *J. Am. Chem. Soc.* **1939**, *61*, 2626.

(64) Hariharan, P. C.; Pople, J. A. *Theor. Chim. Acta* **1973**, *28*, 213.

(65) Wofford, B. A.; Bevan, J. W.; Olson, W. B.; Lafferty, W. J. *Chem. Phys. Lett.* **1986**, *124*, 579.

C–H stretch is a normal mode for the monomer and for all polymers in which it is embedded. If Q measures displacement along this coordinate from the monomer equilibrium bond length, then the potential energy surface for a C–H stretching vibration within a cluster will have the form

$$V = sQ + \tfrac{1}{2}kQ^2 + \tfrac{1}{6}tQ^3 + \ldots \qquad \text{(A1)}$$

This assumption implies that there are no coupling terms to other coordinates.

Now if

$$\Delta V = sQ + \tfrac{1}{6}tQ^3 \qquad \text{(A2)}$$

is regarded as a perturbation to the harmonic oscillator potential, the energy and wave function may be expanded as double series in s and t:

$$\psi_n = \sum_{j,k} \psi_{jkn} s^j t^k \qquad \text{(A3)}$$

$$E_n = \sum_{j,k} E_{jkn} s^j t^k \qquad \text{(A4)}$$

The coefficients in these expansions, ψ_{jkn} and E_{jkn}, may be evaluated by using perturbation theory. Because E_{10n} is zero, the leading correction to the transition energy, $\Delta\Delta E = \Delta(E_1 - E_0)$, due to the formation of a polymer is

$$\Delta\Delta E = (E_{111} - E_{110})st \qquad \text{(A5)}$$

provided one makes the second assumption that $t \gg s$. The perturbation sums are evaluated to give

$$\Delta\Delta E = -stE_{000}/k^2 \qquad \text{(A6)}$$

To lowest order in s, the values of t and k in this expression may consistently be replaced by their values for the free monomer. The third major assumption of the electrostatic model is that s may be evaluated accurately from electrostatics provided the polymer geometry is given.

In the electrostatic model one evaluates the average value of sQ with the monomer anharmonic wave function:

$$\Delta\Delta E = \langle \psi_{100} + t\psi_{101} | sQ | \psi_{100} + t\psi_{101} \rangle / (1 + t^2 \langle \psi_{101} | \psi_{101} \rangle) - \langle \psi_{000} + t\psi_{001} | sQ | \psi_{000} + t\psi_{001} \rangle / (1 + t^2 \langle \psi_{001} | \psi_{001} \rangle) \qquad \text{(A7)}$$

The zeroth-order terms in this expression are zero, so the leading term is st. By interchange perturbation theory this term has the same value as found above from the double series.

In the ab initio approach, a new equilibrium value for Q is found. Under the assumptions made here this will be $Q_e = -s/k$ to lowest order. Then a new harmonic force constant is computed

$$k' = (\partial^2 V/\partial Q^2)_e = k - st/k \qquad \text{(A8)}$$

Finally, a new harmonic transition energy is computed from

$$\Delta\Delta E = 2E_{000}(k'/k)^{1/2} = 2E_{000}(1 - st/k^2)^{1/2} \qquad \text{(A9)}$$

To the first approximation this gives once again, the expression of eq A6.

As is obvious from this derivation, the electrostatic model can easily fail in situations where the ab initio model will still perform well. In particular, our normal-coordinate analysis has demonstrated that the C–H stretching modes become strongly coupled in $(HCN)_3$. The electrostatic model assumption requiring the invariance of the modes with polymerization is therefore inappropriate. The failure of the assumption that s can be evaluated from electrostatics can account for the poor agreement of the calculated $(HCN)_2$ shifts with those observed. The ab initio calculations, not being tied to these assumptions, have reproduced the shifts rather well.

Registry No. HCN, 74-90-8; $(HCN)_2$, 24993-07-5; $(HCN)_3$, 81751-48-6; $(HCN)_4$, 27072-02-2.

Extended X-ray Absorption Fine Structure Studies of Platinum–Tin Catalysts

G. Meitzner, G. H. Via, F. W. Lytle,[†] S. C. Fung, and J. H. Sinfelt*

Corporate Research Laboratories, Exxon Research and Engineering Company, Annandale, New Jersey 08801

(Received: October 7, 1987)

Extended X-ray absorption fine structure (EXAFS) studies at 140 K, along with studies of X-ray absorption edges themselves, were conducted on a $Pt–Sn/Al_2O_3$ catalyst that had previously been exposed to hydrogen at high temperatures (775–795 K). For comparison, similar studies were conducted on a $Pt–Sn/SiO_2$ sample. For the $Pt–Sn/Al_2O_3$ catalyst the extent of coordination of tin to platinum atoms or to other atoms of tin is small, but the extent of coordination to oxygen is substantial. An analysis of the energy shift of the K absorption edge of the tin indicates that the tin is not present as Sn^{4+}. The EXAFS data, coupled with the absorption edge data, suggest that the tin is largely present as Sn^{2+}. There appears to be a significant interaction between the platinum and tin, since the platinum is more highly dispersed on alumina when tin is present. After consideration of all the data, it seems reasonable to regard the catalyst as if it consisted essentially of platinum clusters dispersed on an alumina that has Sn^{2+} present at the surface. The EXAFS data on the $Pt–Sn/SiO_2$ sample lead to very different conclusions. In this case, most of the tin has an oxidation state of zero, and the material consists predominantly of bimetallic entities of platinum and tin on silica.

Introduction

For almost two decades, bimetallic reforming catalysts have played a major role in the petroleum industry in the production of aromatic hydrocarbons for automotive fuels.[1] Two catalyst systems of early interest in this regard were platinum–rhenium and platinum–iridium. These systems are still widely used in commercial reforming units and have been the subjects of many investigations by research workers in the field of heterogeneous catalysis. Various types of investigations of platinum–iridium catalysts have provided evidence that bimetallic clusters of platinum and iridium are present in such catalysts.[1-4] Extended X-ray absorption fine structure (EXAFS) studies have been es-

---

[†] The Boeing Co., Seattle, WA 98124.

(1) Sinfelt, J. H. *Bimetallic Catalysts: Discoveries, Concepts, and Applications*; Wiley: New York, 1983; pp 130–157.

(2) Sinfelt, J. H. U.S. Patent 3 953 368, 1976.

(3) (a) Sinfelt, J. H.; Via, G. H. *J. Catal.* **1979**, *56*, 1. (b) Garten, R. L.; Sinfelt, J. H. *J. Catal.* **1980**, *62*, 127.

(4) Sinfelt, J. H.; Via, G. H.; Lytle, F. W. *J. Chem. Phys.* **1982**, *76*, 2779.

0022-3654/88/2092-2925$01.50/0